Tetrahedron 69 (2013) 1970–1977

Contents lists available at SciVerse ScienceDirect

Tetrahedron

journal homepage: www.elsevier.com/locate/tet

Efficient organic dyes containing dibenzo heterocycles as conjugated linker part for dye-sensitized solar cells

Shengyun Cai, Xiaohao Hu, Jinlong Han, Zhiyun Zhang, Xin Li, Chengyou Wang, Jianhua Su *

Key Laboratory for Advanced Materials and Institute of Fine Chemicals, East China University of Science & Technology, Shanghai 200237, China

ARTICLE INFO

Article history:
Received 6 November 2012
Received in revised form 23 December 2012
Accepted 31 December 2012
Available online 8 January 2013

Keywords:
DSSCs
Dibenzo
Heterocycles
Dibenzofuran
Dibenzothiophene

ABSTRACT

Six new organic dyes, **TBS1**–**TBS6**, have been synthesized and characterized by optical, electrochemical, and theoretical studies. Among these dyes, DSSCs based on a dye containing *N*-hexylcarbazole and furan moieties (**TBS4**) showed the best performance, with light-to-electricity conversion efficiency up to 5.91% under AM 1.5 solar simulator, much higher than the reference dye **TPS** (4.24%). The high V_{oc} contributed to the good performance for **TBS4**, which may be ascribed to the combined effects of twisted structure and hexyl chain. Additionally, for **TBS4** based DSSCs, under optimized conditions, the light-to-electricity conversion efficiency was enhanced up to 7.09%. The results suggest that dibenzo heterocycles containing dyes are promising candidates for application in DSSCs.

1. Introduction

Since the pioneering report by O'Regan and Grätzel in 1991,[1] dye-sensitized solar cells (DSSCs) have received extensive interest because of their easy processing, low cost, high solar energy to electricity conversion efficiency (η), and potential application in the industry.[2] Although the DSSCs based on ruthenium(II) polypyridyl complexes exhibited a record high conversion efficiency over 11%: **N3**, **N719**, and the black dye,[3–5] there are many deficits to counteract, such as high cost, the use of noble metal, and difficulties in synthesis and purification.[6] Recently, much attention is directed to the development of metal-free organic dyes owing to the advantages of environmental friendliness, higher structural flexibility, lower cost, and easier preparation.[2b,7] A large number of organic dyes for use as molecular photovoltaics have been designed and synthesized. Due to the effective photoinduced intramolecular charge-transfer characteristics, most of the efficient organic sensitizers are modeled on the donor–(π-spacer)– acceptor (D–π–A) system.[8,9] Among others, the structure of the π spacer is one of the crucial factors that influence the conversion efficiency of solar energy into electricity in DSSCs. Herein, we report our efforts on the design of different π conjugated linkers.

Triphenylamine is an excellent donor, however, due to the good planarity between the donor and π spacer, many sensitizers based on triphenylamine donor generally can produce fluorescence emission and the corresponding DSSCs exhibited unfavorable dye aggregation and fast charge recombination between the oxidized dyes and the injected electrons.[9,10] Many attempts were made to increase the dihedron angles appropriately between the donor and π spacer without hugely breaking the π conjugation of the dye molecule. Previously, it was reported that the inserting of a fluorene unit between triarylamine unit and thiophene moiety could result a relative large dihedron angle.[10d] Because dibenzo heterocycles, such as carbazole, dibenzofuran, and dibenzothiophene have the similar structure as fluorene, thus the inserting of dibenzo heterocycles units between triphenylamine unit and thiophene moiety could also be expected to twist the dye molecule. Based on the above ideas, we have developed six new dyes (Scheme 1) for DSSCs using triphenylamine as donor, carbazole (or dibenzofuran or dibenzothiophene) connected with thiophene or furan as π-spacer and 2-cyno acetic acid as acceptor based on the following considerations: (1) the direct linkage of carbazole unit with triphenylamine was found to not only increase the electron-donating ability but also reinforce the hole-transporting capabilities, which promote the charge separation.[11,12] Besides, this kind of structure was found to improve the morphological stability of the films in OLEDs.[11,12] Thus, similar effect could be expected to be produced in DSSCs; (2) the insertion of carbazole (or dibenzofuran or dibenzothiophene) unit between the triphenylamine unit and thiophene (or furan) unit may twist the dye molecule thus result in appropriate deviation of a sensitizer molecule from planarity, which

---

* Corresponding author. Tel./fax: +86 21 64252288; e-mail address: bbsjh@ecust.edu.cn (J. Su).

0040-4020/$ – see front matter © 2013 Elsevier Ltd. All rights reserved.
http://dx.doi.org/10.1016/j.tet.2012.12.074

could avoid dye aggregation and/or close contact of electrolyte molecules with the TiO_2. As a result, a high V_{oc} could be anticipated; (3) dibenzofuran and dibenzothiophene are excellent charge carriers and electron transporters,[12b–f] however, very few of sensitizers have employed these structures as conjugated π-spacers in DSSCs, not to mention the systematic research on them. Here, by changing carbazole unit for dibenzofuran or dibenzothiophene moiety, thus the effects of the insertion of three kinds of moieties on the performance of DSSCs based on these dyes could be systematically investigated; (4) thiophene could result in the bathchromic shift of the absorption spectrum, and furan can provide more effective conjugation and lower the energy of the charge-transfer transition, thus the photovoltaic performance for the dyes with the two π-spacers could be compared with.[9e,12a,13,14] Based on the above considerations, herein, we report the synthesis, characterization, optical properties and electrochemical characteristics of the six new organic dyes.

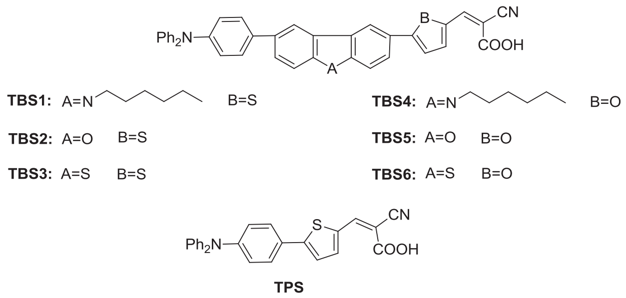

Scheme 1. Molecular structures of the dyes **TBS1**–**TBS6** and **TPS**.

2. Results and discussion

2.1. Synthesis

The synthetic route to the six dyes **TBS1**–**TBS6** is depicted in Scheme 2. The synthesis of these compounds started from triphenylamine, which was used to prepare (4-(diphenylamino)phenyl) boronic acid according to previous report.[17] The three key intermediates **4a**–**c** were easily obtained from commercially available materials carbazole, dibenzofuran and dibenzothiophene via bromination reaction, respectively, according to the paper.[15,16] Asymmetrical Suzuki coupling reaction of compound **4a**–**c** with 4-(diphenylamino)phenylboronic acid gave white compounds **5a**–**c**. Then Suzuki coupling of **5a**–**c** with 5-formylthiophene- 2-boronic acid or 5-formylfuran-2-boronic acid, respectively, afforded monoaldehyde-substituted precursors **6a**–**f**. The final products **TBS1**–**TBS6** were obtained via Knoevenagel condensation with cyanoacetic acid in the presence of a catalytic amount of piperidine in THF. Compound **TPS** was synthesized by using a literature procedure.[17] The purification of intermediates was performed by flash column chromatography and subsequent HPLC. All the intermediates and target dyes were characterized by standard spectroscopic methods including ^1H NMR, ^{13}C NMR, and HRMS. Clearly, all the intermediates and target compounds are stable.

2.2. Optical properties

UV/Vis absorption spectra of the seven dyes in a diluted solution of THF are shown in Fig. 1 and their absorption data are listed in Table 1. In the UV/Vis spectra, the dyes **TBS1**–**TBS6** and **TPS** all exhibit one major and broad absorption band at 350–600 nm with the maximum absorption at 422, 406, 414, 442, 384, 407, and 443 nm, respectively. The corresponding maximum molar extinction coefficients are 2.14×10^4, 2.86×10^4, 2.80×10^4, 2.70×10^4, 2.30×10^4, 2.02×10^4, and 2.51×10^4 M^{-1} cm^{-1}. The absorption band was ascribed to the intramolecular charge-transfer (**ICT**) between the donor and the acceptor. It is obvious that **TBS2** have higher molar extinction coefficients and red-shifted absorption spectra compared with **TBS5**, which may be due to the introduction of the thiophene instead of furan moiety. The red-shifted phenomenon may be ascribed to the different aromatic ability of the two five-membered heteroaromatic bridges. The aromatic of furan is larger than that of thiophene due to the stronger electronegative of oxygen element than that of sulfur element. It could be seen that the λ_{max} values in the visible light region shift to a lower energy with the decreased electronegativity of the heteroatoms, which is in accordance with results reported previously.[9e,13,14,18] The comparison of **TBS3** and **TBS6** displayed the same phenomenon. Except **TBS4**, all these dyes display obvious blue-shifted absorption spectra compared with **TPS**, which could be explained by that the introduction of dibenzo heterocycles moiety between thiophene (or furan) and triphenylamine may twist the molecule thus lead to larger dihedral angles between donor and thiophene moiety and make less conjugation for the whole molecule. Among these dyes, **TBS4** exhibits the broadest absorption band in visible light region and high molar extinction coefficient, thus more visible light could be harvested and a high J_{sc} could be expected.

The absorption spectra of **TBS1**–**TBS6** on thin transparent films (4 μm thick) after 12 h adsorption in THF solution are shown in Fig. 2. The maximum absorption peaks for **TBS1**–**TBS6** on the TiO_2 films are located at 409, 392, 394, 410, 379, and 399 nm, correspondingly blue-shifted by 13, 14, 20, 32, 5, 8 nm, respectively, from

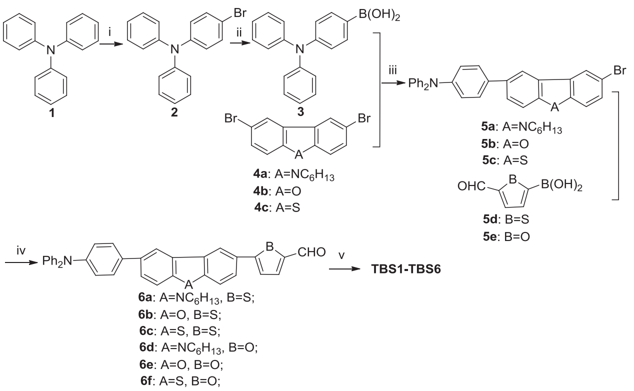

Scheme 2. Synthetic routes of the dyes **TBS1**–**TBS6**. (i) NBS, CCl_4; (ii) (a) BuLi, THF; (b) $B(OiPr)_3$; (c) 2 N HCl (aq); (iii) $Pd(PPh_3)_4$, K_2CO_3,THF; (iv) $Pd(PPh_3)_4$, K_2CO_3,THF; (v) THF, 2-cyanoacetic acid, piperidine.

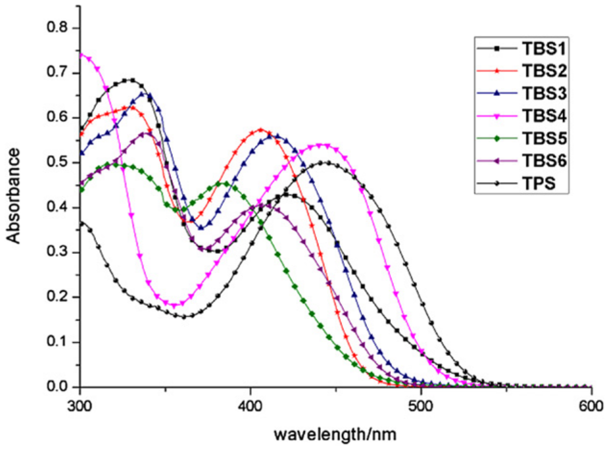

Fig. 1. UV/Vis absorption spectra of **TBS1**–**TBS6** and **TPS** in THF (2×10^{-5} mol/L).

Table 1
Optical and electrochemical data of **TBS1**–**TBS6** and **TPS**

Dye	λ_{max}[a]/nm $\varepsilon/10^4$ M^{-1} cm^{-1})	λ_{max}[b]/nm on TiO_2	Φ_f[a,c]	$E_{0\text{-}0}$[d]	E_{HOMO}[e] (V)	E_{LUMO}[f] (V)
TBS1	422(2.14)	409	0.028	2.38	0.89	−1.49
TBS2	406(2.86)	392	0.0076	2.60	1.00	−1.60
TBS3	414(2.80)	394	0.0022	2.48	0.91	−1.57
TBS4	442(2.70)	410	0.0098	2.36	0.88	−1.48
TBS5	384(2.30)	379	0.0045	2.70	0.98	−1.72
TBS6	407(2.02)	399	0.0065	2.52	0.89	−1.63
TPS	443(2.51)	414	0.54	2.38	1.04	−1.34

[a] Recorded in THF.

[b] Absorption maximum on TiO_2 transparent films.

[c] Florescence quantum yields with rhodamine B (Φ_f=0.70) in ethanol as a standard.

[d] $E_{0\text{-}0}$ of dyes was estimated from the absorption thresholds from absorption spectra of dyes adsorbed on the TiO_2 film.

[e] HOMOs were measured in CH_3CN, scan rate=100 mVs^{-1}; electrolyte=$(n\text{-}C_4H_9)_4NPF_6$; potentials were calibrated with ferrocene/ferrocenium (Fc/Fc^+) as an external reference.

[f] LUMO energy levels were estimated by subtracting E_{0-0} from the HOMO energy level. NHE=normal hydrogen electrode.

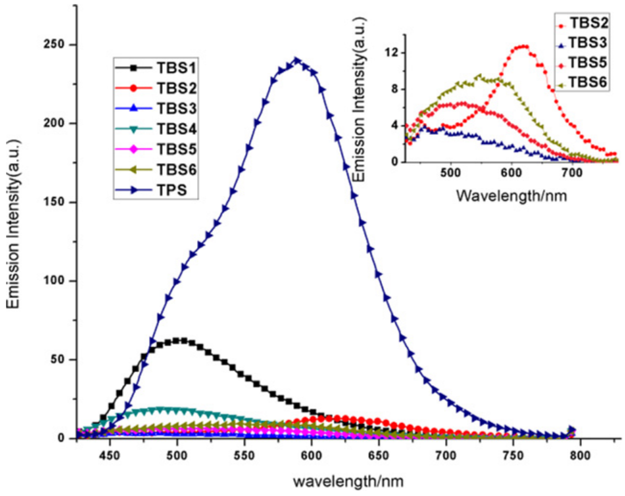

Fig. 3. Emission spectra of dyes in THF (1×10^{-5} mol/L).

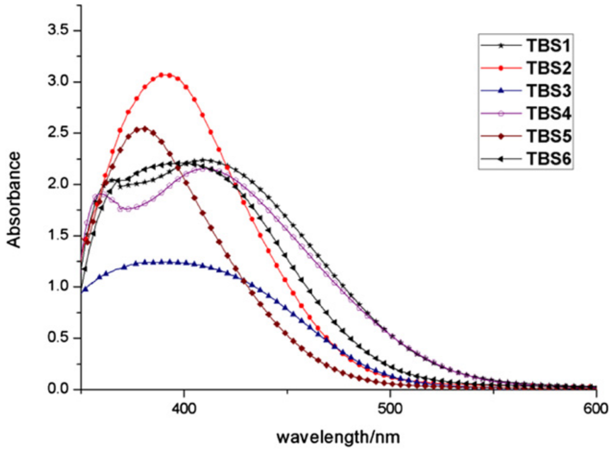

Fig. 2. UV/Vis absorption spectra of **TBS1**–**TBS6** adsorbed on TiO_2 films.

the solution spectra. The blue shift of the absorption spectra of **TBS1**–**TBS6** on TiO_2 could be ascribed to deprotonation of carboxylic acid upon adsorption onto the TiO_2 surface and formation of H-aggregates.[9e,14,19,20] Noted that compared with carbazole containing dyes, the onset wavelengths of dibenzofuran (or dibenzothiophene) containing dyes on TiO_2 films are blue-shifted obviously, which is consistent with the situation that the dyes in THF solution. The emission spectra of **TBS1**–**TBS6** and **TPS** in a diluted solution of THF are in Fig. 3 and the fluorescent quantum yield data are listed in Table 1. It could be easily observed that the dyes **TBS1**–**TBS6** are almost non-emissive while **TPS** displayed obvious fluorescence emission, suggesting that the inserting of carbazole (or dibenzofuran or dibenzothiophene) twists the molecule and suppresses the light emission thus decreases the energy loss.

2.3. Electrochemical properties

To estimate the feasibility of electron-transfer from the excited-state of the dyes to the conduction band of TiO_2 electrode, we carried out cyclic voltammetry experiments in order to determine the redox potentials. The redox potentials of the seven dyes, **TBS1**–**TBS6** and **TPS** were measured in CH_3CN using 0.1 M tetrabutylammonium hexafluorophosphate as the supporting electrolyte, Pt as the counter electrode and a saturated calomel electrode (SCE) as reference electrode. The SCE reference electrode was calibrated using a ferrocene/ferrocenium (Fc/Fc^+) redox couple as an external standard. The electrochemical data for the seven dyes are shown in Fig. S2 (see in the Supplementary data) and summarized in Table 1. HOMO levels of **TBS1**–**TBS6** and **TPS** dyes adsorbed on TiO_2 films corresponding to their first redox potential were determined to be 0.89, 1.00, 0.91, 0.88, 0.98, 0.89, and 1.04 V vs NHE, respectively, which were sufficiently more positive than the iodine/iodide redox potential value (0.4 V), indicating that the oxidized dyes formed after electron injection into the conduction band of TiO_2 could thermodynamically accept electrons from I^- ions. It was easily found that inserting a furan unit instead of a thiophene unit close to the acceptor group slightly promotes the HOMO level, such as **TBS4** and **TBS1**. The higher HOMO level of **TBS4** compared to **TBS1** indicates that **TBS4** is much easier to give electrons. LUMO levels of **TBS1**–**TBS6** and **TPS** dyes are much more negative than that of the conduction band of TiO_2 (−0.5 V vs NHE). Generally, a minimal driving force of 0.2 V is sufficient to ensure fast excited-state injection and regeneration of the oxidized dye.[22] Thus, the excited-state electrons injection of all seven dyes are guaranteed to be efficient. It is noteworthy that LUMO levels of **TBS1**–**TBS6** were much more negative than that of **TPS**, meaning that **TBS1**–**TBS6** have more driving force to inject electrons into the conduction band of TiO_2.

2.4. Computational analysis

To gain insight into the molecular structure, the three-dimensional geometries of the compounds were optimized using density functional theory (DFT) at the B3LYP/6-31G* level of theory.[23] The Gaussian 03 program package was used to carry out the calculations. As shown in Scheme 3, in the ground state the geometry of the dyes is not planar. For **TBS1**–**TBS3**, which contain a thiophene moiety, the molecules are mainly twisted at two positions: One is located between the phenyl ring attached on the nitrogen atom from the triphenylamine unit and the phenyl ring from the carbazole (or dibenzofuran or dibenzothiophene) unit and the dihedral angles are 36.8°, 35.5°, and 35.7°, respectively, the other is located between the phenyl ring from the carbazole (or dibenzofuran or dibenzothiophene) unit and thiophene moiety and the corresponding dihedral angles are 25.3°, 23.5°and 24.1°. However, for **TBS4**–**TBS6**, only one place is twisted, which is located between the phenyl ring attached on the nitrogen atom from the triphenylamine unit and the phenyl ring from the carbazole (or dibenzofuran or dibenzothiophene) unit and the dihedral angles are 37.0°, 35.5°, 36.4°. It is clear that inserting a thiophene unit instead of a furan moiety close to the acceptor can twist the whole molecule more thus decrease the conjugation of the molecule to some extent. One explanation for the larger angles between carbazole (or dibenzofuran or dibenzothiophene) moiety and thiophene moiety compared to the angle between carbazole and furan moieties is that the steric hindrance arose from larger sulfur atom is more pronounced.[9e] Compared with **TPS**, the molecules of the **TBS1**–**TBS6** are twisted more, which facilitates them to prevent the formation of excimer and/or aggregates. The non-planar shape of these dyes due to the existence of carbazole (or dibenzofuran or dibenzothiophene) may also reduce the degree of electronic resonance between D and A.[24] In the process of photoexcitation, one key to increase the device efficiency is to reduce the rate of internal charge recombination. The non-planar geometry between D and A may help to slow down the rate, therefore higher V_{oc} could be expected.

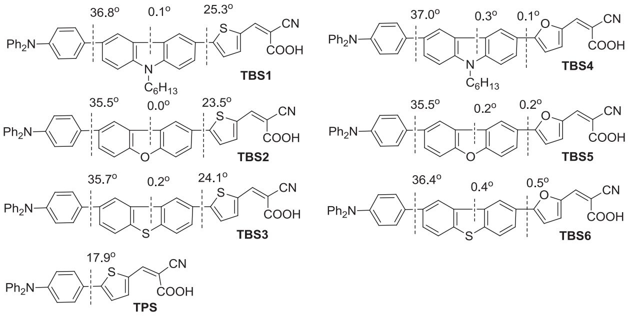

Scheme 3. Dihedral angles of the neighboring aromatic rings for **TBS1**–**TBS6** and **TPS**.

2.5. DSSCs performance

The DSSCs were prepared by using dye-adsorbed TiO_2 electrode, Pt-coated glass as a counter electrode, and an acetonitrile solution with iodine (0.05 M), lithium iodide (0.1 M), 1,2-dimethyl-3-propylimidazolium iodide (0.6 M), and 4-*tert*-butylpyridine (0.5 M) as electrolyte. Fig. 4 shows the action spectra of incident photon-to-current conversion efficiency (IPCE) for DSSCs with these dyes when THF was used as the solvent for dye loading. The IPCE exceeds 60% in the range 395–525 nm for **TBS1**, 355–465 nm for **TBS2**, 350–485 nm for **TBS3**, 375–545 nm for **TBS4**, 355–475 nm for **TBS5**, and 355–500 nm for **TBS6** with the highest value of 71.4% at 500 nm for **TBS1**, 76.3% at 410 nm for **TBS2**, 76.3% at 400 nm for **TBS3**, 83.9% at 490 nm for **TBS4**, 75.2% at 400 nm for **TBS5**, and 83.3% at 450 nm for **TBS6**, respectively. However, the highest value of IPCE for **TPS** was only 63.0% at 470 nm, much lower than that for **TBS1**–**TBS6**. Note that compared to the absorption spectra of sensitized films, the IPCE spectra were broaden significantly. This phenomenon could be ascribed to the scattering effect of the large particles in the film and the reflective effect of the Pt counter electrode. Moreover, the electrolyte could also pose influence on the IPCE values. The IPCE performances of the DSSCs with carbazole containing dyes are better than that of the corresponding dibenzofuran (or dibenzothiophene) containing dyes due to their broader photocurrent action spectrum. The IPCE performance of the **TBS1** device is poorer than that the **TBS4** device due to its narrower photocurrent action spectrum and lower IPCE values, which may be ascribed to the lower molar extinction coefficients. Obviously, with broadest spectra of IPCE and almost the highest values of IPCE, **TBS4** sensitized TiO_2 electrode would generate a higher conversion yield compared to other six dyes.

The photocurrent–voltage (*J*–*V*) plots of DSSCs fabricated with these dyes, along with that of **TPS** for comparison, are shown in Fig. 5. The detailed parameters, i.e., short circuit current (J_{sc}), open-circuit photovoltage (V_{oc}), fill factor (*FF*), and solar-to-electricity conversion efficiency (η) measured under AM 1.5 solar light (100 mW cm^{-2}) are summarized in Table 2. When THF was used as the solvent for dye baths, the DSSCs based on **TBS1**–**TBS6** and **TPS** dyes exhibited inferior conversion efficiency of 5.29%, 3.03%, 3.84%, 5.91%, 3.36%, 4.21%, and 4.25%. From these data, it is clear that the DSSCs based on **TBS1**–**TBS6** dyes all had much higher V_{oc} than that based on **TPS** just as expected. Noticeably, DSSCs based on dyes containing furan moiety correspondingly displayed lager J_{sc} and thus higher conversion efficiency than based on dyes containing thiophene moiety, such as **TBS4** and **TBS1**, which could be ascribed to broader spectra of IPCE and higher IPCE values. Clearly, DSSCs based on **TBS1** exhibited higher V_{oc}, larger J_{sc} thus enhanced conversion efficiency than that based on **TPS**, suggesting that inserting a carbazole unit between the triphenylamine unit and thiophene moiety close to the acceptor could significantly increase the V_{oc} without decreasing the J_{sc}. The performances of the DSSCs based on the dyes containing dibenzofuran or dibenzothiophene moieties were poorer than that the corresponding dyes containing the carbazole moieties. The lower J_{sc} and lower V_{oc} should be responsible for it. The lower J_{sc} for dibenzofuran (or dibenzothiophene) containing dyes could be ascribed to the poorer IPCE performances compared with the DSSCs based on the corresponding dyes

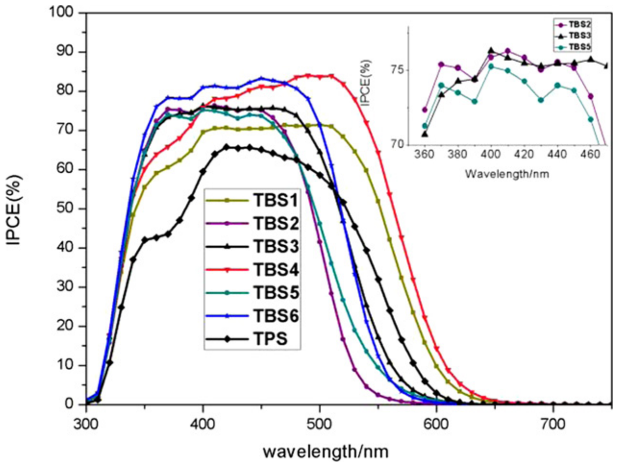

Fig. 4. IPCE spectra of DSSCs based on **TBS1**–**TBS6** and **TPS** when THF was used as the solvent for dye baths.

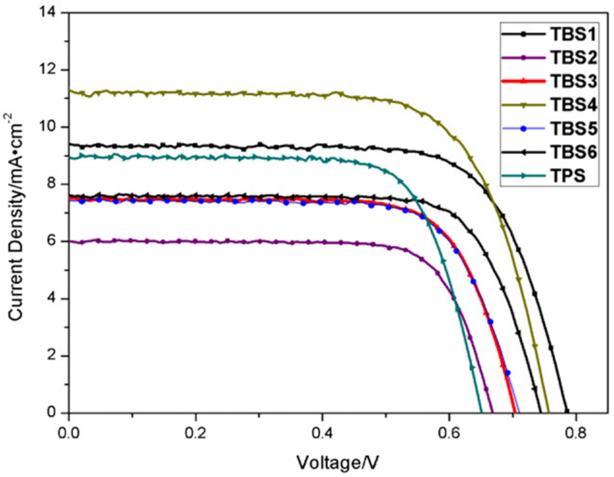

Fig. 5. *J*–*V* curves of DSSCs based on **TBS1**–**TBS6** and **TPS** with dye baths in THF.

Table 2
Photovoltaic performance parameters of the DSSCs based on **TBS1**–**TBS6** and **TPS**

Dye	Solvents[a]	J_{sc}/mA cm^{-2}	V_{oc}/V	*FF* (%)	E_{ff} (%)
TBS1	THF	9.36	0.786	71.8	5.29
TBS2	THF	6.02	0.669	75.2	3.03
TBS3	THF	7.50	0.704	72.7	3.84
TBS4	THF	11.2	0.757	69.5	5.91
TBS5	THF	6.83	0.666	73.9	3.36
TBS6	THF	7.59	0.745	74.5	4.21
TPS	THF	8.97	0.652	72.7	4.25
TBS1	CH_3CN	11.09	0.730	68.6	5.56
TBS1	CH_2Cl_2	9.69	0.771	65.9	4.92
TBS1	^{i}PrOH	7.81	0.755	64.0	3.78
TBS4	CH_3CN	11.8	0.770	0.698	6.33
TBS4	CH_2Cl_2	10.9	0.735	0.681	5.46
TBS4	^{i}PrOH	10.7	0.756	0.700	5.43
TBS4[b]	CH_3CN	13.89	0.769	0.664	7.09

[a] Solvents employed for dye baths for TiO_2 sensitization.

[b] DSSCs fabricated with 16 μm thick 13 nm sized TiO_2 nanoparticles (T/SP).

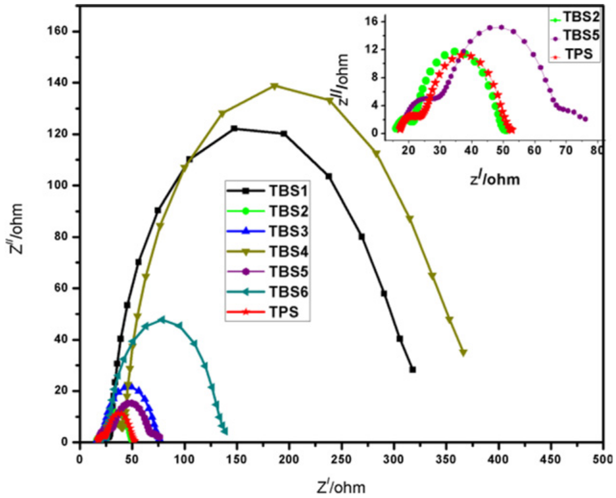

Fig. 6. Nyquist plots of impedance spectra for the DSSCs based on these dyes with dye baths in THF.

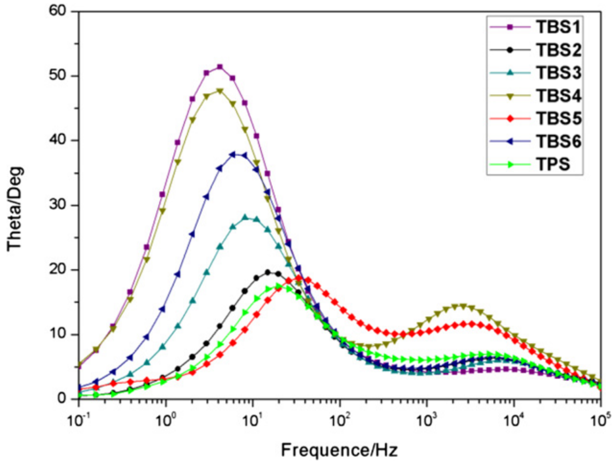

Fig. 7. Bode phase plots of the impedance spectra for the DSSCs based on these dyes with dye baths in THF.

containing carbazole moieties. The lower V_{oc} may be indicative of more severe charge recombination between the electrolytes and the oxidized dyes compared with the DSSCs based on the corresponding dyes containing carbazole moieties. The DSSCs based on **TBS1** displayed poorer performance than that based on **TBS4**, which could be attributed to the much lower J_{sc}. The DSSCs based on **TBS4** displayed the best performance with high V_{oc}, large J_{sc} and relatively low *FF* corresponding to an overall efficiency of 5.91%. In different solvents, dyes exhibit diversified interactions with the solvents and could cause changes of the physical and chemical properties between the dyes and semiconductor surface.[9a,21,24,25] To investigate the effect of solvents on dye baths for TiO_2 sensitization, **TBS1** and **TBS4** in different solvents were employed to sensitize TiO_2. The photovoltaic performance for DSSCS based on **TBS1** and **TBS4** were tested and shown in Table 2. The table reveals that the performances of **TBS1** based DSSCs were all lower than that **TBS4** based DSSCs when used the same solvents for dye baths, which is in accordance with the situation that employed THF as the solvent for dye baths. It could be seen that the two dyes based DSSCs both displayed best when CH_3CN was used as the solvent for dye baths. Noted that **TBS4** based DSSCs fabricated with dye baths in CH_3CN exhibit the best performance with η enhanced up to 6.33%. The enhanced J_{sc} is responsible for the good device performance, which may be resulted from the increased amount of dyes adsorbed on TiO_2 films because of the interaction between the dyes and the solvent, what's more, with dye baths in CH_3CN, the DSSCs made of thicker films of 13 nm sized TiO_2 nanoparticles (T/SP) exhibited the solar-to-electricity conversion efficiency of 7.09% (see Fig. S4 and Fig. S5 in the Supplementary data) due to boomed J_{sc}. The enhancement of J_{sc} could be also ascribed to the increased amount of dyes adsorbed on TiO_2 films because of thicker films of TiO_2.

2.6. Electrochemical impedance spectroscopy

To further elucidate the photovoltaic properties of these dyes, electrochemical impedance spectroscopy (EIS) was performed. EIS analysis of the DSSCs made with these sensitizers were carried out in the dark under a forward bias of −0.70 V. The Nyquist plots of the DSSCs based on the seven dyes under a forward bias of −0.70 V with a frequency range of 0.1 Hz–100 kHz are shown in Fig 6. The Bode phase plots are also shown in Fig. 7. Two semicircles were observed in the Nyquist plots. The smaller semicircle at high frequency is assigned to the redox charge-transfer response at the Pt/electrolyte interface. The large one at the intermediate frequency represents the electron-transfer impedance at the TiO_2/dye/electrolyte interface. The charge recombination resistance at the TiO_2 surface (R_{rec}), it can be deduced by fitting curves from a range of intermediate frequencies using *Z*-view software. It is related to the charge recombination rate, e.g., a smaller R_{rec} indicates a faster charge recombination and therefore a larger dark current (shown in Fig. S3 in the Supplementary data). The radius of the biggest semicircle R_{rec} values decreased in the order of **TBS1**≈**TBS4**>**TBS6**>**TBS3**>**TBS5**>**TBS2**≈**TPS**. The result appears to be roughly consistent with the increase of V_{oc} in the DSSCs based on **TBS1**–**TBS6** and **TPS**. In Bode phase plots, the peak position of the middle frequency is related to the electron lifetime, for example, a shift to low frequency corresponds to a longer electron lifetime. Thus, according to Fig. 7, the order of the corresponding electron lifetimes **TBS1**≈**TBS4**>**TBS6**>**TBS3**>**TBS2**≈**TBS5**>**TPS** further approximately support the order of the V_{oc} of DSSCs based on these dyes. From these data, it could be concluded that the DSSCs based on the dyes of **TBS1**–**TBS6** with the inclusion of carbazole (or dibenzofuran or dibenzothiophene) show slower charge recombination and longer electron lifetime, which contributes to much higher $V_{oc.}$ Noted that carbazole containing dyes exhibited much higher V_{oc} than the dibenzofuran or dibenzothiophene containing dyes. The possible reason is that the attachment of hexyl on the carbazole moiety may suppress the dye aggregation and intermolecular charge recombination further.

3. Conclusion

In summary, three different dibenzo heterocycles units (carbazole, dibenzofuran, and dibenzothiophene) are introduced into π-spacer section and six new metal-free organic dyes (**TBS1**–**TBS6**) based on D–π–A structure were successfully synthesized and demonstrated as efficient sensitizers for DSSCs. The results showed that the inserting of carbazole (or dibenzofuran or dibenzothiophene) appropriately twists the molecule thus decreases the energy loss caused by fluorescence emission. More importantly, the twisted structure slowed down intermolecular charge recombination, as a result, high V_{oc} were obtained. It is noteworthy that the inserting of carbazole (or dibenzofuran or dibenzothiophene) moiety elevated the HOMO levels of the dyes so that all the dyes have strong donating abilities. Among these seven dyes, the DSSCs based on **TBS4** exhibited the best performance with an overall efficiency of 5.91%, much higher than that **TPS** (4.24%) under the same condition. The good device performance could be interpreted by reinforced donating ability, low emission, high electron injection efficiency and low intermolecular charge recombination rate. Additionally, with an optimized dye baths for TiO_2 sensitization and thicker film of TiO_2 nanoparticles (T/SP), the J_{sc} was obviously enhanced, as a result, η of the DSSCs based on **TBS4** was improved to 7.09%. The increase of the J_{sc} may be resulted from the increase of amount of dyes adsorbed on TiO_2 films caused by the interaction between the dyes and solvents and thicker films. However, the performances of the DSSCs based on the dyes containing dibenzofuran or benzothiophene moieties were poorer than that the **TPS** based DSSCs. This could be explained by that the narrower absorption spectra resulted in the corresponding poorer IPCE performances, which contributed to lower J_{sc}. On the other hand, the absence of attachment of a hexyl chain on the dibenzofuran (or dibenzothiophene) moiety contributed to more severe charge recombination between the electrolyte and the oxidized dyes, thus resulted in lower V_{oc} compared with carbazole containing dyes based DSSCs. By the insertion of electron-deficient π spacer, it will improve the conjugation extent of the dye molecule and would be a good try to enhance the device performance for the DSSCs based on these dyes.

4. Experimental section

4.1. Materials and reagents

Optically transparent FTO conducting glass (fluorine doped tin oxide overlayer, transmission >90% in the visible, sheet resistance 15 Ω square^{-1}), Titania pastes of Ti-Nanoxide T/SP and Ti-Nanoxide 300 were obtained from Geao Science and Educational Co. Ltd. of China. Tetra-*n*-butylammonium hexafluorophosphate ($TBAPF_6$), 4-*tert*-butylpyridine (TBP), 2.4 M BuLi solution in hexane and the reaction catalyst $Pd(PPh_3)_4$ were obtained from J&K. Lithium iodide, 1,2-dimethyl-3-propylimidazolium iodide were from Fluka and iodine, 99.999%, was from Alfa Aesar. Acetonitrile with HPLC purity was purchased from SK Chemicals. THF was pre-dried over sodium and distilled under argon atmosphere from sodium benzophenone ketyl immediately prior to use. All other chemicals were used as received without further purification. The starting materials 3,6-dibromo-9-hexyl-9*H*-carbazole, 2,8-dibromodibenzo[*b*,*d*]furan, and 2,8-dibromodibenzo[*b*,*d*]thiophene were synthesized by the previous reported procedures.

4.2. Instruments and characterization

The new compounds were characterized by NMR and Mass. NMR spectra were obtained on a Brucker AM 400 spectrometer and Mass spectra were recorded on an ESI mass spectrometer. The UV–vis absorption spectra of the dyes in solution and adsorbed on TiO_2 films were obtained from a Varian Cary 500 spectrophotometer. The cyclic voltammograms of dyes were measured with a Versastat II electrochemical workstation (Princeton applied research) using a normal three-electrode cell with a Pt working electrode, a Pt wire counter electrode, and a regular calomel reference electrode in saturated KCl solution. The electrochemical impedance spectroscopy (EIS) measurements of all the DSSCs were performed using a Zahner IM6e Impedance Analyzer (ZAHNER-Elektrik GmbH & CoKG, Kronach, Germany).

Photovoltaic measurements were carried out by an AM 1.5 solar simulator equipped with a 300 W xenon lamp (Model No. 91160, Oriel). The power of the simulated light was calibrated to 100 mW cm^{-2} using a Newport Oriel PV reference cell system (Model 91160V). Cell active area was tested with a mask of 0.25 cm^{-2}. The photocurrent action spectra were measured with an IPCE test system consisting of a model SR830 DSP Lock. In Amplifier and a model SR540 Optical Chopper (Stanford Research Corporation, USA), a 7IL/PX150 xenon lamp and power supply, and a 7ISW301 spectrometer.

4.3. Synthesis

*4.3.1. 5-(7-(4-(Diphenylamino)phenyl)-9-hexyl-9H-carbazol-3-yl) thiophene-2-carbaldehyde (**6a**).* In a 100 mL three-necked round-bottom flask, compound **5a** obtained above (1.2 g, 2.0 mmol), K_2CO_3 (1.38 g, 10 mmol), $Pd(PPh_3)_4$ (50 mg, 0.05 mmol), water (5 mL), and THF (10 mL) were heated to 45 °C for 1 h under an argon atmosphere. Then, (4-formylphenyl)boronic acid (468 mg, 3.0 mmol) dissolved in 10 mL THF was added and the reaction was stirred at 45 °C for 4 h. The mixture was washed with water and extracted with chloroform. The combined organic layer was dried over anhydrous $MgSO_4$ and concentrated using a rotary evaporator. The residue was purified by column chromatography on silica (petroleum ether/dichloromethane=1:2, v/v) to yield the product as a yellow powder (360 mg, 30%). ^{1}H NMR (400 MHz, $CDCl_3$): 9.89 (s, 1H), 8.44 (d, *J*=1.5 Hz, 1H), 8.33 (s, 1H), 7.83–7.76 (m, 2H), 7.74 (d, *J*=8.5 Hz, 1H), 7.61 (d, *J*=8.5 Hz, 2H), 7.50–7.42 (m, 3H), 7.30 (d, *J*=8.1 Hz, 4H), 7.20 (d, *J*=8.5 Hz, 2H), 7.17 (d, *J*=7.7 Hz, 4H), 7.04 (t, *J*=7.3 Hz, 2H), 4.34 (t, *J*=7.2 Hz, 2H), 1.95–1.86 (m, 2H), 1.36–1.28 (m, 6H), 0.87 (t, *J*=7.0 Hz, 3H). ^{13}C NMR (DMSO-d_6, 100 MHz), δ: 182.63, 156.32, 147.82, 146.62, 141.48, 141.22, 140.27, 137.95, 136.01, 132.67, 129.29, 127.93, 125.63, 124.63, 124.57, 124.41, 124.26, 124.15, 123.57, 123.16, 118.62, 118.56, 109.43, 109.37, 43.44, 31.57, 29.02, 26.98, 22.56. HRMS (*m*/*z*): $[M]^+$ calcd for $C_{41}H_{37}N_2OS$, 605.2627; found, 605.2631.

*4.3.2. Compound **6b**–**f**.* Compound **6b**–**f** was synthesized by the same procedure as described for **6a**. Compound **6b**: ^{1}H NMR (400 MHz, $CDCl_3$): 9.91 (s, 1H), 8.27 (d, *J*=1.7 Hz, 1H), 8.17 (d, *J*=1.5 Hz, 1H), 7.79 (d, *J*=8.5 Hz, 1H), 7.71 (dd, *J*=8.5,1.5 Hz, 1H), 7.63 (d, *J*=8.6 Hz, 3H), 7.56 (d, *J*=8.5 Hz, 2H), 7.47 (d, *J*=3.9 Hz, 1H), 7.29 (t, *J*=7.8 Hz, 5H), 7.20 (d, *J*=8.5 Hz, 2H), 7.16 (d, *J*=8.1 Hz, 4H), 7.05 (t, *J*=7.2 Hz, 2H). ^{13}C NMR (DMSO-d_6, 100 MHz), δ: 182.72, 154.36, 147.63, 147.54, 147.44, 142.37, 141.17, 138.46, 137.92, 137.51, 136.31, 135.55, 134.68, 129.67, 129.35, 128.05, 126.50, 125.02, 124.50, 124.16, 119.68, 119.29. HRMS (*m*/*z*): $[M]^+$ calcd for $C_{35}H_{24}NO_2S$, 522.1528; found, 522.1528. Compound **6c**: ^{1}H NMR (400 MHz, $CDCl_3$): 9.92 (s, 1H), 8.47 (d, *J*=1.5 Hz, 1H), 8.37 (d, *J*=1.4 Hz, 1H), 7.91 (dd, *J*=8.3, 1.9 Hz, 2H), 7.81–7.70 (m, 3H), 7.60 (d, *J*=8.6 Hz, 2H), 7.53 (d, *J*=3.9 Hz, 1H), 7.30 (t, *J*=7.9 Hz, 4H), 7.19 (dd, *J*=16.0, 8.1 Hz, 6H), 7.06 (t, *J*=7.3 Hz, 2H). ^{13}C NMR (DMSO-d_6, 100 MHz), δ: 182.75, 157.21, 156.10, 154.52, 147.68, 147.22, 142.28, 137.63, 136.48, 134.90, 129.34, 128.25, 128.07, 127.01, 125.96, 125.31, 124.45, 123.01, 118.84, 118.74, 112.50, 112.03. HRMS (*m*/*z*): $[M]^+$ calcd for $C_{35}H_{24}NOS_2$, 538.1299; found, 538.1296. Compound **6d**: ^{1}H NMR (400 MHz, $CDCl_3$): 9.64 (s, 1H), 8.64 (d, J=1.4 Hz, 1H), 8.37 (d, J=1.5 Hz, 1H), 7.93 (dd, J=8.6, 1.6 Hz, 1H), 7.74 (dd, J=8.5, 1.7 Hz, 1H), 7.61 (d, J=8.6 Hz, 2H), 7.46 (t, J=8.3 Hz, 2H), 7.37 (d, J=3.7 Hz, 1H), 7.31–7.26 (m, 4H), 7.19 (dd, J=13.8, 8.1 Hz, 6H), 7.04 (t, J=7.3 Hz, 2H), 6.86 (d, J=3.7 Hz, 1H), 4.34 (t, J=7.2 Hz, 2H), 1.96–1.86 (m, 2H), 1.46–1.30 (m, 6H), 0.87 (t, J=7.0 Hz, 3H). ^{13}C NMR (DMSO-d_6, 100 MHz), δ: 176.67, 161.28, 151.58, 147.83, 146.62, 141.61, 140.22, 135.98, 132.71, 129.28, 127.90, 125.52, 124.40, 124.27, 123.49, 123.44, 120.06, 118.73, 117.96, 109.34, 109.26, 106.15, 43.43, 31.55, 29.02, 26.97, 22.55, 14.02. HRMS (m/z): $[M]^+$ calcd for $C_{41}H_{37}N_2O_2$, 589.2855; found, 589.2858. Compound **6e**: ^{1}H NMR (400 MHz, $CDCl_3$): 9.67 (s, 1H), 8.50 (d, J=1.6 Hz, 1H), 8.20 (d, J=1.6 Hz, 1H), 7.92 (dd, J=8.6, 1.8 Hz, 1H), 7.72 (dd, J=8.6, 1.8 Hz, 1H), 7.63 (dd, J=8.6, 4.8 Hz, 2H), 7.57 (d, J=8.6 Hz, 2H), 7.37 (d, J=3.7 Hz, 1H), 7.32–7.27 (m, 5H), 7.20 (d, J=8.6 Hz, 2H), 7.17 (d, J=7.6 Hz, 4H), 7.05 (t, J=7.3 Hz, 2H), 6.90 (d, J=3.7 Hz, 1H). ^{13}C NMR (DMSO-d_6, 100 MHz), δ: 177.02, 159.72, 157.31, 156.05, 151.92, 147.68, 147.20, 136.46, 134.85, 129.34, 128.02, 126.92, 125.17, 124.98, 124.45, 123.00, 118.91, 117.92, 112.39, 112.00, 107.23. HRMS (m/z): $[M]^+$ calcd for $C_{35}H_{24}NO_3$, 506.1756; found, 506.1741. Compound **6f**: ^{1}H NMR (400 MHz, $CDCl_3$): 9.69 (s, 1H), 8.69 (s, 1H), 8.45 (d, J=1.5 Hz, 1H), 7.91 (d, J=8.2 Hz, 3H), 7.74 (s, 1H), 7.63 (d, J=8.6 Hz, 2H), 7.39 (d, J=3.7 Hz, 1H), 7.32–7.28 (m, 4H), 7.20 (dd, J=16.8, 8.1 Hz, 6H), 7.07 (d, J=7.3 Hz, 2H), 6.97 (d, J=3.7 Hz, 1H). ^{13}C NMR (DMSO-d_6, 100 MHz), δ: 177.06, 159.65, 152.00, 147.66, 147.41, 141.45, 138.30, 137.98, 136.20, 135.68, 134.68, 129.34, 128.11, 126.41, 125.51, 124.48, 124.01, 123.81, 119.92, 118.27, 107.68. HRMS (m/z): $[M]^+$ calcd for $C_{35}H_{24}NO_2S$, 522.1528; found, 522.1524.

*4.3.3. 5-(4-(Diphenylamino)phenyl)thiophene-2-carbaldehyde (**6g**).* The procedure is similar as the procedure for the synthesis of **6a**. The yield: 45%.

*4.3.3.1. (Z)-2-Cyano-3-(5-(7-(4-(diphenylamino)phenyl)-9-hexyl-9H-carbazol-3-yl)thiophen-2-yl)acrylic acid (**TBS1**).* A mixture of **6a** (300 mg, 0.5 mmol), 2-cyanoacetic acid (160 mg, 2 mmol) and 2 drops of piperidine in 20 ml THF was refluxed for 4 h under N_2 atmosphere. After cooled to rt, the solvent was removed in vacuo. The residual was dissolved in 200 ml dichloromethane and washed with redistilled water for three times. The combined organic layer was dried over anhydrous $MgSO_4$ and then filtered. The filtrate was concentrated using rotary evaporator. The crude product was chromatographed on silica gel and firstly using pure dichloromethane as the eluent to exclude the impurities and then using THF and methanol mixture (1:1) as the eluent to obtain the pure product as an orange solid (301 mg, 90%). ^{1}H NMR (400 MHz, DMSO-d_6): 8.67 (d, J=1.6 Hz, 1H), 8.61 (d, J=1.5 Hz, 1H), 8.19–8.09 (m, 1H), 7.88–7.81 (m, 1H), 7.81–7.74 (m, 4H), 7.72–7.65 (m, 3H), 7.37–7.31 (m, 4H), 7.13–7.04 (m, 8H), 4.57–4.32 (m, 2H), 1.91–1.71 (m, 2H), 1.35–1.20 (m, 6H), 0.81 (t, J=7.1 Hz, 3H). ^{13}C NMR (DMSO-d_6, 100 MHz), δ: 156.32, 152.43, 151.10, 145.96, 145.11, 142.62, 140.64, 139.96, 136.47, 134.76, 132.95, 130.15, 129.46, 129.26, 129.17, 128.97, 128.44, 128.14, 127.90, 123.88, 123.34, 115.41, 115.20. HRMS (m/z): $[M]^+$ calcd for $C_{44}H_{38}N_3O_2S$, 672.2685; found, 672.2681.

*4.3.4. Compounds **TBS2**–**6** and **TPS**.* Compound **TBS2**–**6** and **TPS** were synthesized by the same procedures as described above for **TBS1** using corresponding carbaldehyde (**6b**–**f**). Compound **TBS2**: ^{1}H NMR (400 MHz, DMSO-d_6): 8.64 (d, J=1.8 Hz, 1H), 8.56 (d, J=1.6 Hz, 1H), 8.50 (s, 1H), 8.03 (d, J=4.1 Hz, 1H), 7.94 (dd, J=8.7, 1.9 Hz, 1H), 7.80 (dt, J=7.4, 2.5 Hz, 3H), 7.72 (dd, J=14.0, 8.6 Hz, 3H), 7.37–7.31 (m, 4H), 7.08 (m, 8H). ^{13}C NMR (DMSO-d_6, 100 MHz), δ: 163.65, 156.43, 155.34, 152.92, 147.05, 146.52, 146.46, 141.39, 135.45, 134.45, 134.06, 129.55, 127.95, 127.76, 126.56, 126.02, 124.98, 124.74, 123.99, 123.74, 119.41, 119.24, 116.54, 112.63, 111.98. HRMS (m/z): $[M]^+$ calcd for $C_{38}H_{25}N_2O_3S$, 589.1586; found, 589.1587. Compound **TBS3**: ^{1}H NMR (400 MHz, DMSO-d_6): 8.99 (d, J=1.6 Hz, 1H), 8.84 (d, J=1.4 Hz, 1H), 8.51 (s, 1H), 8.16–8.06 (m, 3H), 7.97 (d, J=4.0 Hz, 1H), 7.87 (dd, J=8.4, 1.8 Hz, 1H), 7.84–7.77 (m, 3H), 7.35 (t, J=7.9 Hz, 4H), 7.14–7.06 (m, 8H). ^{13}C NMR (DMSO-d_6, 100 MHz), δ: 153.01, 147.03, 146.73, 141.29, 140.31, 137.72, 136.82, 136.35, 136.00, 133.91, 129.58, 129.16, 128.09, 126.00, 125.41, 125.03, 124.01, 123.51, 123.45, 123.18, 120.20, 119.74, 116.54. HRMS (m/z): $[M]^+$ calcd for $C_{38}H_{25}N_2O_2$, 605.1357; found, 605.1354. Compound **TBS4**: ^{1}H NMR (400 MHz, DMSO-d_6): 13.58 (s, 1H), 8.88 (d, J=1.4 Hz, 1H), 8.41 (s, 1H), 8.11–8.04 (m, 2H), 7.84–7.77 (m, 2H), 7.71 (dd, J=11.5, 8.7 Hz, 3H), 7.61 (d, J=3.8 Hz, 1H), 7.38–7.31 (m, 5H), 7.12 (d, J=8.6 Hz, 2H), 7.08–7.06 (m, 6H), 4.47 (t, J=6.8 Hz, 2H), 1.80 (d, J=6.9 Hz, 2H), 1.37–1.23 (m, 6H), 0.8 (t, J=7.1 Hz, 3H). ^{13}C NMR (DMSO-d_6, 100 MHz), δ: 164.21, 160.67, 147.19, 146.83, 145.98, 141.23, 139.86, 137.44, 135.28, 131.28, 131.58, 129.52, 127.60, 125.20, 124.03, 123.79, 122.94, 122.58, 119.52, 118.08, 117.97, 117.06, 110.28, 110.21, 108.29, 95.36, 42.55, 30.91, 28.53, 26.06, 21.97, 13.80. HRMS (m/z): $[M]^+$ calcd for $C_{44}H_{38}N_3O_3$, 656.2913; found, 656.2909. Compound **TBS5**: ^{1}H NMR (400 MHz, DMSO-d_6): 8.69 (d, J=1.1 Hz, 1H), 8.32 (s, 1H), 8.03 (dd, J=8.7, 1.6 Hz, 1H), 7.91 (s, 1H), 7.79 (dd, J=12.1, 5.1 Hz, 2H), 7.74 (d, J=8.6 Hz, 1H), 7.67 (d, J=8.6 Hz, 5H), 7.35 (d, J=8.0 Hz, 3H), 7.32 (d, J=2.6 Hz, 2H), 7.26 (d, J=3.6 Hz, 1H), 7.10 (d, J=3.3 Hz, 2H), 7.09 (d, J=0.6 Hz, 4H), 7.06 (s, 2H). ^{13}C NMR (DMSO-d_6, 100 MHz), δ: 156.32, 156.00, 155.27, 148.29, 147.03, 146.58, 135.50, 134.08, 129.57, 127.92, 124.59, 124.35, 124.16, 124.04, 123.77, 123.48, 123.16, 118.68, 117.51, 112.44, 112.04, 108.52. HRMS (m/z): $[M]^+$ calcd for $C_{38}H_{25}N_2O_4$, 573.1814; found, 573.1816. Compound **TBS6**: ^{1}H NMR (400 MHz, DMSO-d_6): 9.03 (d, J=1.0 Hz, 1H), 8.66 (d, J=1.2 Hz, 1H), 8.17 (d, J=8.4 Hz, 1H), 8.10 (d, J=8.4 Hz, 1H), 8.07–8.00 (m, 2H), 7.83 (dd, J=8.4, 1.6 Hz, 1H), 7.76 (d, J=8.6 Hz, 2H), 7.48 (s, 2H), 7.35 (t, J=7.9 Hz, 4H), 7.14–7.06 (m, 8H). ^{13}C NMR (DMSO-d_6, 100 MHz), δ: 163.94, 157.55, 147.89, 147.02, 146.84, 140.03, 137.72, 136.81, 135.70, 135.34, 133.71, 129.60, 127.86, 125.98, 125.65, 124.13, 123.85, 123.42, 119.37, 118.52, 117.85, 109.50. HRMS (m/z): $[M]^+$ calcd for $C_{38}H_{25}N_2O_3S$, 589.1586; found, 589.1582.

Supplementary data

Supplementary data related to this article can be found online at http://dx.doi.org/10.1016/j.tet.2012.12.074.

References and notes

1. O'Regan, B.; Grätzel, M. *Nature* **1991**, *353*, 737–740.
2. (a) Hagfeldt, A.; Grätzel, M. *Chem. Rev.* **1995**, *95*, 49–68; (b) Zhou, H. P.; Xue, P. C.; Zhang, Y.; Zhao, X.; Jia, J. H.; Zhang, X. F.; Liu, X. L.; Lu, R. *Tetrahedron* **2011**, *67*, 8477–8483; (c) Chou, H.-H.; Hsu, C.-Y.; Hsu, Y.-C.; Lin, Y.-S.; Lin, J. T.; Tsai, C. *Tetrahedron* **2012**, 767–773.
3. Green, M. A.; Emery, K.; Hishikawa, Y.; Warta, W. *Prog. Photovolt. Res. Appl.* **2008**, *16*, 61–67.
4. (a) Nazeeruddin, M. K.; Kay, A.; Rodicio, L.; Humphry-Baker, R.; Müller, E.; Liska, P.; Vlachopoulos, N.; Grätzel, M. *J. Am. Chem. Soc.* **1993**, *115*, 6382–6390; (b) Grätzel, M. *J. Photochem. Photobiol., A* **2004**, *164*, 3–14; (c) Fillaut, J. L.; Perruchon, J.; Blanchard, P.; Roncali, J.; Golhen, S.; Allain, M.; Migalska-Zalas, A.; Kityk, I. V.; Sahraoui, B. *Macromol. Rapid Commun.* **2007**, *28*, 1761–1775.
5. (a) Nazeeruddin, M. K.; Zakeeruddin, S. M.; Humphry-Baker, R.; Jirousek, M.; Liska, P.; Vlachopoulous, N.; Shklover, V.; Fischer, C. H.; Grätzel, M. *Inorg. Chem.* **1999**, *38*, 6298–6305; (b) Perruchon, J.; Blanchard, P.; Roncali, J.; Golhen, S.; Allain, M.; Misgalsaka-Zalas, A.; Kityk, I. V.; Saharaoui, B. *Organometallics* **2005**, *24*, 687–695.
6. (a) Chen, C.-Y.; Wu, S.-J.; Wu, C.-G.; Chen, J.-G.; Ho, K.-C. *Angew. Chem.* **2006**, *118*, 5954–5957 *Angew. Chem., Int. Ed.* **2006**, *45*, 5822–5825; (b) Chen, C.-Y.; Wu, S.-J.; Li, J.-Y.; Wu, C.-G.; Chen, J.-G.; Ho, K.-C. *Adv. Mater.* **2007**, *19*, 3888–3891; (c) Gao, F.; Wang, Y.; Zhang, J.; Shi, D.; Wang, M.; Humphry-Baker, R.; Wang, P.; Zakeeruddin, S. M.; Grätzel, M. *Chem. Commun.* **2008**, 2635–2637; (d) Chen, C.-Y.; Chen, J.-G.; Wu, S.-J.; Li, J.-Y.; Wu, C.-G.; Ho, K.-C. *Angew. Chem.* **2008**, *120*, 7452–7455 *Angew.Chem., Int. Ed.* **2008**, *47*, 7342–7345.
7. (a) Ito, S.; Zakeeruddin, M.; Hummphrey-Baker, R.; Liska, P.; Charvet, R.; Comte, P.; Nazeeruddin, M. K.; Pchy, P.; Takata, M.; Miura, H.; Uchida, S.; Grätzel, M. *Adv. Mater.* **2006**, *18*, 1202–1205; (b) Zhang, G.; Bala, H.; Cheng, Y.; Shi, D.; Lv, X.; Yu, Q.; Wang, P. *Chem. Commun.* **2009**, 2198–2200; (c) Jia, J. H.; Cao, K. Y.; Xue, P. C.; Zhang, Y.; Lu, R. *Tetrahedron* **2012**, *68*, 3626–3632; (d) Tian, H. N.; Yang, X. C.; Chen, R. K.; Pan, Y. Z.; Li, L.; Hagfeldt, A.; Sun, L. C. *Chem. Commun.* **2007**,

3741–3743; (e) Enger, O.; Nuesh, F.; Fibbioli, M.; Echegoyen, L.; Pretsch, E.; Diederich, F. *J. Mater. Chem.* **2000**, *10*, 2231–2233.

8. (a) Chang, Y. J.; Chou, P.-T.; Lin, S.-Y.; Watanabe, M.; Liu, Z.-Q.; Lin, J.-L.; Chen, K.-Y.; Sun, S.-S.; Liu, C.-Y.; Chow, T. J. *Chem.—Asian J.* **2012**, *7*, 572–581; (b) Kim, S.; Choi, H.; Baik, C.; Song, K.; Kang, S. O.; Ko, J. *Tetrahedron* **2007**, *63*, 11436–11443; (c) Cheng, X. B.; Liang, M.; Sun, S. Y.; Shi, Y. B.; Ma, Z. J.; Sun, Z.; Xue, S. *Tetrahedron* **2012**, *68*, 5375–5385.
9. (a) Chang, Y.-J.; Chow, T.-J. *J. Mater. Chem.* **2011**, *21*, 9523–9531; (b) Zhao, Y.; Ye, C. Q.; Qiao, Y. L.; Xu, W.; Song, Y. L.; Zhu, D. B. *Tetrahedron* **2012**, *68*, 1547–1551; (c) Cho, N.; Kim, J.; Song, K.; Lee, J. K.; Ko, J. *Tetrahedron* **2012**, *68*, 4029–4036; (d) Chang, Y. J.; Chow, T. J. *Tetrahedron* **2009**, *65*, 4726–4734; (e) Chaurasia, S.; Chen, Y.-C.; Chou, H.-H.; Wen, Y.-S.; Lin, J. T. *Tetrahedron* **2012**, *68*, 7755–7762; (f) Tian, H. N.; Yang, X. C.; Chen, R. K.; Zhang, R.; Hagfeldt, A.; Sun, L. C. *J. Phys. Chem. C* **2008**, *112*, 11023–11033.
10. (a) Chen, Y.-C.; Chen, Y.-H.; Chou, H.-H.; Chaurasia, S.; Wen, Y. S.; Lin, J.-T.; Yao, C.-F. *Chem.—Asian J.* **2012**, *7*, 1074–1084; (b) Cocherel, N.; Leriche, P.; Ripaud, E.; Gallego-Planas, N.; Frere, P.; Roncali, J. *New J. Chem.* **2009**, *33*, 801–806; (c) Hagberg, D. P.; Marinado, T.; Boschloo, G.; Hagfeldt, A.; Sun, L. C. *Chem. Commun.* **2006**, 2245–2247; (d) Li, W. Q.; Wu, Y. Z.; Li, X.; Xie, Y. S.; Zhu, W. H. *Energy Environ. Sci.* **2010**, *4*, 1830–1837.
11. (a) Zhang, Q.; Chen, J.; Chen, Y.; Wang, L.; Ma, D.; Jing, X.; Wang, F. *J. Mater. Chem.* **2004**, *14*, 895–900; (b) Li, J.; Ma, C.; Tang, J.; Lee, C.; Lee, S. *Chem. Mater.* **2005**, *17*, 615–619; (c) Li, J.; Liu, D.; Li, Y.; Lee, C.; Kwong, H.; Lee, S. *Chem. Mater.* **2005**, *17*, 1208–1212; (d) Hu, N.; Xie, S.; Popovic, Z.; Ong, B.; Hor, A. *J. Am. Chem. Soc.* **1999**, *121*, 5097–5098; (e) Hu, N.; Xie, S.; Popovic, Z. D.; Ong, B.; Hor, A. *Synth. Met.* **2000**, *111–112*, 421–424.
12. (a) Thomas, K. R. J.; Kapoor, N.; Lee, C.-P.; Ho, K.-C. *Chem.—Asian J.* **2012**, *7*, 738–750; (b) Oh, S.; Lee, K. H.; Kim, Y. K.; Yoohn, S. S. *Mater. Res. Bull.* **2012**, *47*, 2792–2795; (c) Jeong, S. H.; Lee, J. Y. *Org. Electron.* **2012**, *13*, 1141–1145; (d) Jeong, S. H.; Lee, J. Y. *Org. Electron.* **2012**, *13*, 2589–2593; (e) Dong, S.-C.; Gao, C.-H.; Zhang, Z.-H.; Jiang, Z.-Q.; Lee, S.-T.; Liao, L. S. *Phys. Chem. Chem. Phys.* **2012**, *14*, 14224–14228; (f) May, F.; Al-Helwi, M.; Baumeier, B.; Kowalsky, W.; Fuchs, E.; Lennartz, C.; Andreniko, D. *J. Am. Chem. Soc.* **2012**, *134*, 13818–13822.
13. (a) Mao, J. Y.; Guo, F. L.; Ying, W. J.; Wu, W. J.; Li, J.; Hua, J. L. *Chem.—Asian J.* **2012**, *7*, 982–991; (b) William, K.; Zhang, Y.; Aebersold, A.; Araujo de Castro, F.; Geiger, T.; Heier, J.; Kuster, S.; Ma, C.-Q.; Bauerle, P.; Nuesch, F.; Tisserant, J.-N.; Hany, R. *Org. Electron.* **2012**, *13*, 1204–1212.
14. (a) Sakong, C.; Kim, S. H.; Yuk, S. B.; Namgoong, J. W.; Park, S. W.; Ko, M. J.; Kim, D. H.; Hong, K. S.; Kim, J. P. *Chem.—Asian J.* **2012**, *7*, 1817–1826; (b) Shen, P.; Liu, X. P.; Jiang, S. H.; Huang, Y. S.; Yi, L.; Zhao, B.; Tan, S. T. *Org. Electron.* **2011**, *12*, 1992–2002; (c) Wang, L.; Wang, H. Y.; Fang, H. H.; Wang, H.; Yang, Z. Y.; Gao, B. R.; Chen, Q. D.; Han, W.; Sun, H. B. *Adv. Funct. Mater* **2012**, *22*, 2783–2791.
15. Korang, J.; Grither, W. R.; McCull, R. D. *J. Am. Chem. Soc.* **2010**, *132*, 4466–4476.
16. Zhang, S. L.; Chen, R. F.; Yin, J.; Liu, F.; Jiang, H. J.; Shi, N.; An, Z. F.; Ma, C.; Liu, B.; Huang, W. *Org. Lett.* **2010**, *12*, 3438–3441.
17. Tang, J.; Hua, J. L.; Wu, W. J.; Li, J.; Jin, Z. G.; Long, Y. T.; Tian, H. *Energy Environ. Sci.* **2010**, *3*, 1736–1745.
18. Hwang, S.; Lee, J. H.; Park, C.; Lee, H.; Kim, C.; Park, C.; Lee, M. H.; Lee, W.; Park, J.; Kim, K.; Park, N. G.; Kim, C. *Chem. Commun.* **2007**, 4887–4889.
19. Chen, R.; Zhao, G.; Yang, X.; Jiang, X.; Liu, J.; Tian, H.; Gao, Y.; Liu, X.; Han, K.; Sun, M.; Sun, L. *J. Mol. Struct.* **2008**, *876*, 1–8.
20. Tang, Z.-M.; Lei, T.; Jiang, K.-J.; Song, Y.-L.; Pei, J. *Chem.—Asian J.* **2010**, *5*, 1911–1917.
21. Ozawa, H.; Awa, M.; Ono, T.; Arakawa, H. *Chem.—Asian J.* **2012**, *7*, 156–162.
22. Liu, B.; Liu, Q. B.; You, D.; Li, X. Y.; Narutac, Y.; Zhu, W. H. *J. Mater. Chem.* **2012**, *22*, 13348–13356.
23. (a) Becke, A. D. J. *Chem. Phys.* **1993**, *98*, 5648–5652; (b) Hehre, W. J.; Ditchfield, R.; Pople, J. A. J. *Chem. Phys.* **1972**, *56*, 2257–2261.
24. Yang, C.-J.; Chang, Y. J.; Watanabe, M.; Hon, Y.-S.; Chow, T. J. *J. Mater. Chem.* **2012**, *22*, 4040–4049.
25. Robertson, N. *Angew. Chem.* **2006**, *118*, 2398–2405; *Angew. Chem., Int.Ed.* **2006**, *45*, 2338–2345.